Hard carbon porosity revealed by the adsorption of multiple gas probe molecules (N 2 , Ar, CO 2 , O 2 and H 2)

Adrian Beda, Cyril Vaulot, Camélia Ghimbeu

Hard carbon porosity revealed by the adsorption of multiple gas probe molecules (N_2, Ar, CO_2, O_2 and H_2)

*Adrian Beda [abc], Cyril Vaulot [ab] and Camélia Matei Ghimbeu *[abc]*

[a]*Université de Haute-Alsace, Institut de Science des Matériaux de Mulhouse (IS2M), CNRS UMR 7361, F-68100 Mulhouse, France.*

[b]*Université de Strasbourg, F-67081 Strasbourg, France*

[c]*Réseau sur le Stockage Electrochimique de l'Energie (RS2E), CNRS FR3459, 33 Rue Saint Leu, 80039 Amiens Cedex, France*

**E-mail: camelia.ghimbeu@uha.fr; Tel: +33 389608743*

Abstract

The porosity of hard carbon materials is usually assessed by nitrogen adsorption, which can lead to apparently non-porous materials and misleading interpretation of sodium storage in Na-ion batteries. Herein, a series of complementary gases (N_2, Ar, CO_2, O_2 and H_2) were used to reveal the porosity of hard carbons. In particular, unconventional gases, such as H_2 and O_2, showed significantly higher adsorbed volumes and specific surface areas than N_2, Ar or even CO_2. Notably, O_2 was the only gas able to access both the ultramicropores ($d < 0.7$ nm) and supermicropores ($0.7 < d < 2.0$).

Porous and non-porous hard carbon (HC) materials are used in many industrial applications, such as pollution control devices, water and air decontamination, gas filters, catalysis and energy storage.[1–6] Especially, HCs have become the most promising class of anode materials[7–9] used in new emerging technology based on Na-ion batteries (NIBs) owing to their eco-friendly nature, low price and good performance. HCs are derived from the pyrolysis of various precursors and due to their high thermal stability they are able to maintain a disordered structure even at high temperatures (>1500 °C), which is favorable for Na-ion storage.[7] In addition, hard carbons exhibit a high degree of cross-linking and possess a very complex structure composed of a mixture of pseudo-graphitic domains (sp^2-hybridized) and amorphous regions containing sp^3 carbon, which are displayed as "houses of cards", as proposed by the model reported by Dahn et al.[10] Between these graphitic-like structures, open and/or closed nanopores (nanovoids) are formed depending on the synthesis conditions (precursor type and annealing temperature).

Although Na^+ storage in HC materials is still debated in the literature,[8,9] it is commonly accepted that carbon porosity plays a key role in reversible and irreversible storage. Based on the galvanostatic charge/discharge curve shape and several in situ and ex situ techniques, Na^+ was proposed to be stored in carbon nanopores, either at high potential (>0.1 V) in the so-called sloping region, or at low potential (<0.1 V) in the plateau region.[11–15] Moreover, carbon pore size and pore accessibility have of great influence in the adsorption of different molecules, such as water from the atmosphere, solvent and electrolyte, all of which impacting Na^+ storage. The pore volume also dictates the number of species that can be adsorbed at the carbon electrode/electrolyte interface. Moreover, the specific surface area (SSA) that is exposed to the electrolyte is known to induce electrolyte decomposition and the formation of a solid electrolyte interphase (SEI), leading to an undesirable irreversible capacity.[12,16–18] Therefore, accurate determination of the hard carbon porosity is of prime importance for better understanding the complex texture of HCs, their interactions with the electrolyte and their performance.

In most reported studies in the literature, nitrogen (N_2) adsorption at 77 K is commonly used to determine the specific surface area, the total pore volume (V_t), and the pore size distribution (PSD). Thus, very often, hard carbon exhibits low surface area when N_2 adsorption is used.[9] However, it is important to be clearly highlight that N_2 is not trivial as an adsorptive for assessing the narrow and restricted porosity of hard carbon materials. One reason for this is the complex structure of HCs, which include both graphitic and amorphous domains that contribute to the formation of different types of pores, i.e., accessible (open), partially accessible

(restricted pores) or closed.[19] The important quadrupole moment of the nitrogen molecule (which may lead to its interactions with a material's surface functionalities), its larger size and its slow diffusion kinetics,[20,21] are other aspects that contribute to the difficulty of providing a detailed characterization of porosity bellow 2 nm. Kr is recommended for low surface area materials due to its low saturation pressure; however, we have showed that Kr fails to characterize the texture of HCs, resulting in a very low SSA (<1 m^2 g^{-1}).[12] Thus, we proposed that CO_2 gas to be used as a probe molecule and demonstrated that some HC materials contain ultramicropores (pore size < 0.7 nm) that are not accessible by N_2.[12] The higher analysis temperature (273 K) favours the diffusion of CO_2 into the narrow pores leading thus to significant higher specific surface areas than N_2 and Kr.

Despite this finding, carbon dioxide is still marginally used, and consequently, it is difficult to appreciate the true contribution of porosity to Na^+ storage mechanisms on the capacity delivered by HC materials. Ar is recommended by the IUPAC[21] as a better option to N_2 due to its null quadrupole moment, which is especially applicable for PSD evaluation. However, the use of expensive liquid Ar (87 K) as a coolant is less suitable from a cost point of view, and thus measurements in liquid nitrogen (77 K) are often employed. Very recently, O_2 and H_2, which possess low quadrupole moments and limited surface interactions with the functional groups on the material surface, were proposed as interesting alternatives for better characterizing pore size distribution. However, this approach was used for highly porous activated carbons,[22,23] and there have been no studies on hard carbon materials with restricted pores, which are the materials usually used as anodes for Li, Na, and K batteries. Alternatively, some authors used Small Angle X-ray Scattering (SAXS) analyses[13,24,25] to obtain information about the hard carbon pore size. However, such technique is limited to the average pore size determination, other useful textural properties such pore size distribution, pore volume or specific surface area cannot be determined.

Herein, we propose for the first time a systematic assessment of hard carbon texture with conventional (N_2, Ar and CO_2) and unconventional gases (O_2 and H_2). Hard carbon is shown to possess a high porosity that can be accessed in large extent only by O_2 or H_2 and to a lesser extent by CO_2. N_2 and Ar proved to be inefficient gases for characterizing hard carbon ultramicroporosity.

The hard carbon, referred to as HAB-1300, was prepared by hydrothermal carbonization of an aqueous solution of glucose, and the obtained hydrochar was pyrolyzed at 1300 °C in an inert atmosphere, as described in detail in the ESI. The characteristic structure of the hard carbon was determined via several analyses techniques as shown in Fig. 1. The X-ray diffraction (XRD) pattern of the material reveals three broad peaks at ~21.6°, 43.6° and 80°, corresponding to the (002), (100) and (110) diffraction planes of graphite, respectively (Fig. 1a).

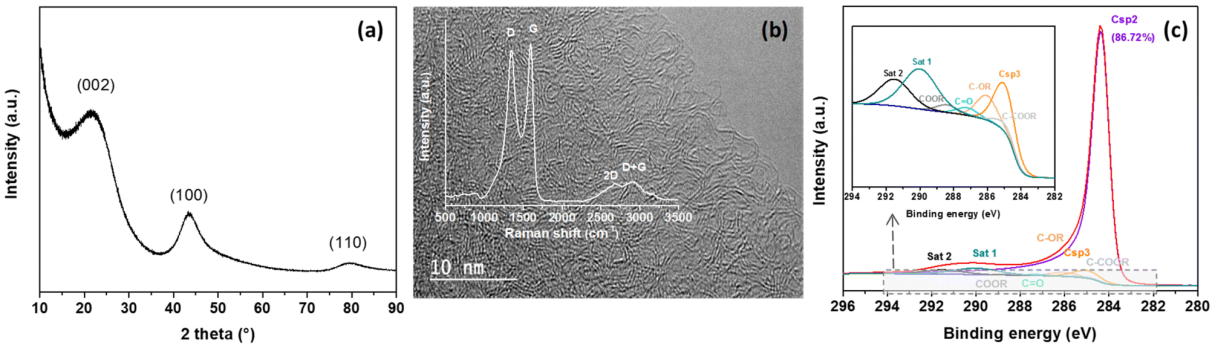

Fig. 1 *XRD pattern (a), an HR-TEM image (b) along with the Raman spectrum (inset) and the XPS C 1s high-resolution deconvoluted spectrum of HAB-1300 hard carbon (c).*

Unlike graphite, HAB-1300 exhibits a low graphitization degree, as indicated by the broad shape of the peaks. The Raman spectrum (inset Fig. 1b) shows two intense and sharp peaks at 1346 cm^{-1} and 1593 cm^{-1}, associated to the defect induced D-band and the crystalline graphite G-band, respectively. The intensity ratio of the two bands (I_D/I_G) is 1.2, which denotes a disordered material. This is in line with the additional broad and low intense peaks (2D and D + G bands) observed at higher Raman shifts (2500–3000 cm^{-1}). The high-resolution transmission electron microscopy (HR-TEM) image (Fig. 1b) shows a mixture of disordered-like carbon and packed curved randomly oriented graphene layers, in accordance with the "house of cards" model proposed by Stevens and Dahn.[26] The high-resolution deconvoluted XPS C 1s spectra of HAB-1300 (Fig. 1c) shows a main contribution of C sp^2 and a negligible contribution of C sp^3. Several types of oxygen-based functional groups can be observed, such as COOR, C–OR, C–COOR and C=O, giving rise to an oxygen content of 2.9 at%. The presence of functional groups might be important for the interaction with adsorbed molecules. For instance, N_2 or CO_2, for which the quadrupole moment grants interactions with different functional groups, may affect both the orientation of the nitrogen molecule on the adsorbent surface (i.e., hard carbon) and the micropore filling pressure.[20] The findings of all these analyses indicate a typical hard carbon structure.

To evaluate the porosity of the material in detail, five different gases were used, and the adsorption–desorption isotherms were measured. The results are presented in linear (Fig. 2a) and semi-logarithmic plots (Fig. 2b) to reveal the differences in the low pressure region where micropore filling occurs.

The results obtained with N_2 and Ar adsorption are very similar (Fig. 2a); however, the material absorbs slightly more N_2 than Ar. This is also revealed by the higher SSA obtained with N_2 (19 $m^2\ g^{-1}$) than with Ar (12 $m^2\ g^{-1}$) (Fig. 2c), as well as by the total pore volume obtained: 0.012 $cm^3\ g^{-1}$ (N_2) vs. 0.007 $cm^3\ g^{-1}$ (Ar). To explain the observed results, first, the size of the molecules can be considered, as their size may hinder penetration into the pores due to steric effects.

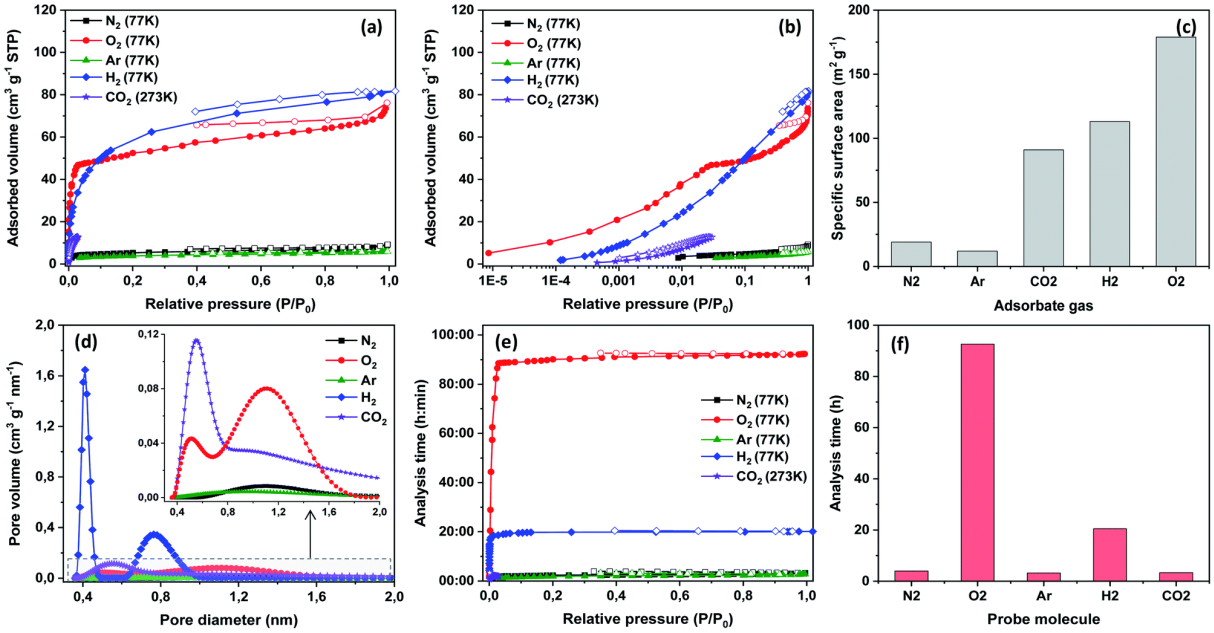

Fig. 2 *Comparison of the adsorption–desorption isotherms obtained from HAB-1300 using different gases; (a) linear view and (b) semi-logarithmic view. In the case of the H_2 adsorption isotherms, since the saturation pressure (P_0) cannot be reached at 77 K, the absolute pressure (P) was divided by the atmospheric pressure (760 mmHg) to obtain P/P_0 to allow better data comparison. (c) Specific surface area evolution with the adsorbate gas and (d) 2D-NLDFT pore size distribution based on different isotherms. (e) Adsorption/desorption isotherms obtained on HAB-1300 hard carbon using different gas probe molecules expressed as analysis time vs. relative pressure. (f) The total time required to perform an adsorption/desorption analysis when different gases were used. The solid symbols indicate adsorption and the open symbols represent desorption.*

As seen in Table 1, the molecular size of N_2 is larger than that of Ar (0.364 vs. 0.340 nm); therefore, this hypothesis can be excluded. In the semi-logarithmic representation of the isotherms (Fig. 2b), one can see that N_2 adsorption starts at a lower relative pressure (8×10^{-3}) than Ar adsorption (3×10^{-2}).

Table 1 *Properties of the adsorbate gases including the molecular size, the quadrupole moment,[27] the polarizability[27,28] and the textural properties, i.e., the specific surface area (SSA), the total pore volume (V_t) and the average pore size (L_0), of the HAB-1300 hard carbon determined by different gas adsorption*

Adsorbate	Molecular size nm	Quadrupole moment $\times 10^{40}$ cm^2	Polarizability $\times 10^{-25}$ cm^3	SSA m^2 g^{-1}	V_t cm^3 g^{-1}	L_0 nm
N_2	0.364	−4.91	17.4	19	0.012	1.87
Ar	0.340	0.00	16.4	12	0.007	1.45
CO_2	0.330	−13.71	29.1	91	0.024	0.94
O_2	0.346	−1.33	15.8	279	0.112	1.22
H_2	0.289	2.2	8.1	113	—	0.52

As argon has no quadrupole moment, no interactions with the oxygen-containing functional groups are expected; therefore, the micropores that are filled with Ar at higher relative pressures have a faster diffusion and a shorter equilibrium time than those filled with N_2. Consequently, Ar can also access slightly smaller pores (down to 0.4 nm) than N_2 (>0.7 nm), as indicated by the pore size distribution (Fig. 2d) obtained using the two-dimensional non-local density function theory (2D-NLDFT).[29] The lower adsorbed Ar volume compared to the adsorbed N_2 volume may be due to the analysis temperature used (77 K), which is below the equilibrium temperature of Ar (87 K).

However, both adsorbed nitrogen and adsorbed argon present limited diffusion through ultramicropores (width < 0.7 nm) at cryogenic temperatures; this phenomenon is a well-known disadvantage of these gases. Specifically, in the case of hard carbons, which are considered non-porous materials in many studies based on nitrogen adsorption results, the evaluation of porosity using CO_2 adsorption has recently[12] demonstrated that a large number of materials contain many ultramicropores. When the CO_2 adsorption experiment is performed at 273 K, the faster diffusion kinetics allow diffusion into very narrow pores. However, due to the high saturation pressure (26. 200 torr), the relative pressure range is limited to $P/P_0 \sim 3 \times 10^{-2}$, whereas the full range can be measured with N_2 and Ar ($P/P_0 = 1$). The results presented in the

linear plot (stars, Fig. 2a) show a significantly higher volume of CO_2 gas than either N_2 (5 cm^3 g^{-1}) or Ar (3 cm^3 g^{-1}) adsorbed at $3 \times 10^{-4} P/P_0$ (13 cm^3 g^{-1}), which is in good agreement with our previous observations.[12,30,31] Thus, a significantly higher SSA is obtained with CO_2 (91 m^2 g^{-1}) than with N_2 (19 m^2 g^{-1}) or Ar (12 m^2 g^{-1}). The semi-logarithmic plot (Fig. 2b) clearly shows that CO_2 adsorption starts at a lower relative pressure ($P/P_0 \sim 4.5 \times 10^{-4}$) than N_2 or Ar adsorption; therefore, CO_2 fills the narrowest micropores at a much lower relative pressure. This is highlighted by the pore size distribution, which reveals much higher pore volume (30 times) by CO_2 adsorption than by N_2 or Ar adsorption (Fig. 2d).

For further analyses, two additional non-conventional gases were explored, namely, O_2 and H_2. These gases have not, to our knowledge, been used before to study the porosity of hard carbon. Moreover, it is possible to use liquid nitrogen as a coolant agent, which is practical from an experimental and cost point of view. H_2 represents a better alternative to CO_2 gas for assessing micro/ultramicroporosity since it has both a smaller quadrupole moment and molecular diameter than CO_2; thus, H_2 might access a smaller range of pores. In addition, at 77 K, hydrogen is supercritical and diffuses faster than CO_2.

Very surprisingly, the adsorption isotherms obtained with either O_2 or H_2 showed significantly higher adsorbed volumes of gas (105 and 82 cm^3 g^{-1} at $P/P_0 = 1.0$) than those obtained with N_2 and Ar (<10 cm^3 g^{-1}). The O_2 and H_2 adsorption/desorption isotherms have a type I shape according to IUPAC classification. The isotherms are characterized by a steep increase in the volume of gas adsorbed at a low relative pressure, followed by a plateau, which is specific for microporous materials. The high adsorbed volumes of O_2 and H_2 suggests that the structure of hard carbon contains a large number of micropores and ultramicropores that are not accessible to conventional gases. The specific surface area (Fig. 2c) is the highest when using O_2 (279 m^2 g^{-1}) followed by H_2 (113 m^2 g^{-1}), CO_2 (93 m^2 g^{-1}) and N_2/Ar (<20 m^2 g^{-1}). A similar trend is observed when using other hard carbons (HPR-1300 and TCA-1400), as demonstrated in Fig. 3 and Table S1 (ESI). We can see that the surface areas of the three HCs determined with N_2 are small and very similar (<25 m^2 g^{-1}), while the surfaces determined with CO_2 or O_2 are significantly larger (up to 431 m^2 g^{-1}), Table S1.

Although the adsorbed volume of O_2 is always higher than that of N_2, important differences among the materials can be observed, highlighting their distinct textures.

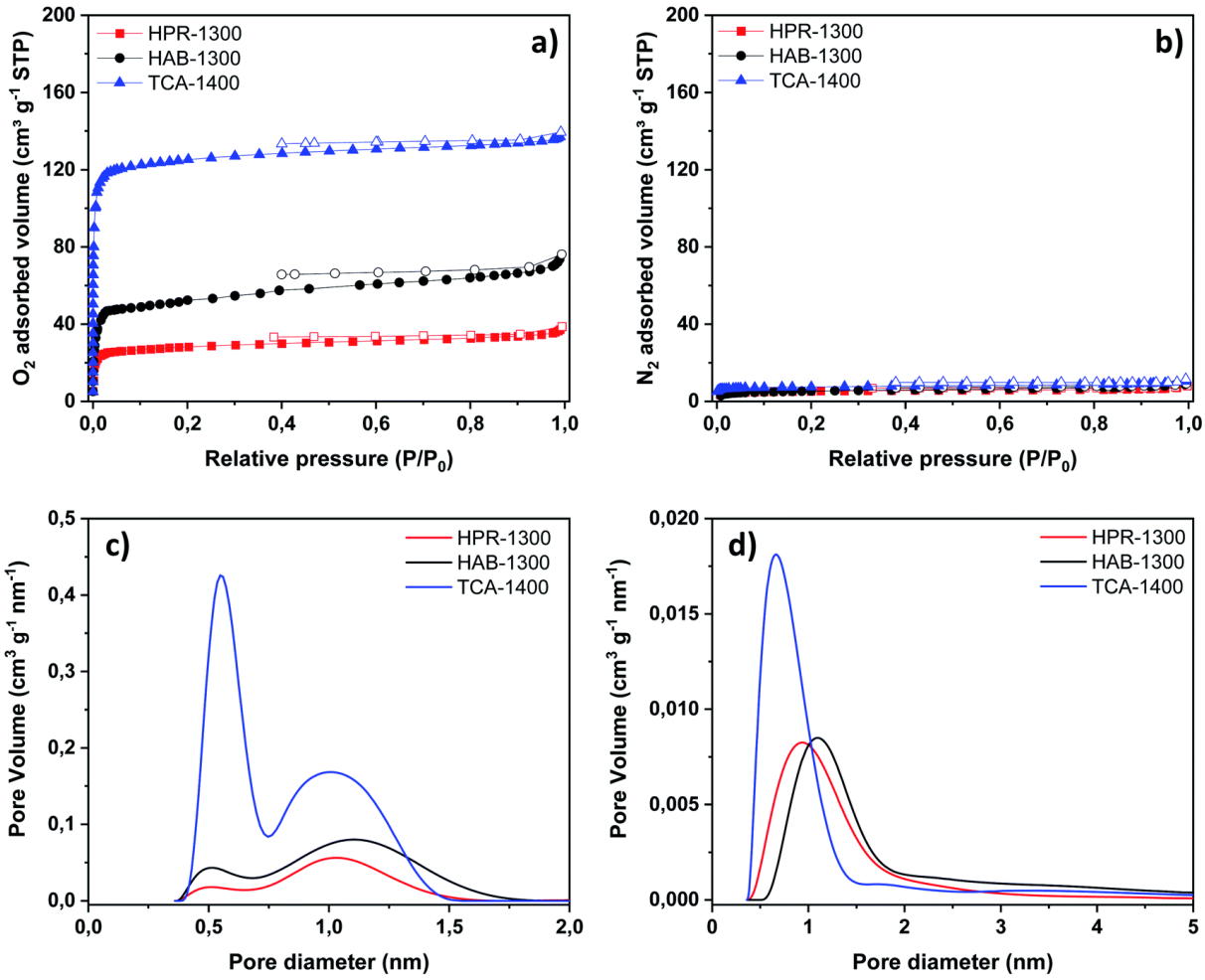

Fig. 3 *Comparison of the (a) O_2 and (b) N_2 adsorption–desorption isotherms obtained on HPR-1300, HAB-1300 and TCA-1400 materials along with (c and d) their corresponding 2D-NLDFT pore size distribution.*

The pore size distribution (Fig. 2d) for O_2 ranged between 0.4 and 1.7 nm, and had two mains peaks at approximately 0.5 nm and 1.1 nm. For CO_2, the PSD is much narrower and centred around 0.55 nm (Fig. 2d). Notably, this peak is placed in the same position as the first peak of O_2, but its intensity is much higher for CO_2 than for O_2, signifying that CO_2 diffuses better in very small pores. This can be related to the high analysis temperature when using CO_2 (273 K) allowing higher diffusion rate in the ultra-micropores (<0.7 nm). However, the high saturation pressure (~26.000 torrs) limits the relative pressure (P/P_0) to 0.03 and thus the possibility to analyse larger pores than 1 nm. Therefore, O_2 appears to be a very appealing gas probe molecule that can access both ultramicropores (d_{pore} < 0.7 nm) and supermicropores (0.7 < d_{pore} < 2 nm), while CO_2 accesses only ultramicropores but in a more efficient manner than O_2. In addition,

H_2 proved to be very interesting in its ability to access very narrow pores, as suggested by the very intense and sharp peak at 0.4 nm and by a second much broader peak at 0.8 nm. The main reason why H_2 can preferentially diffuse in the narrowest pores can be explained by its lower molecular size (0.289 nm) compared to CO_2 (0.33 nm) and O_2 (0.346 nm). However, due to its supercritical conditions at 77 K it cannot condensate, thus, pores larger than 0.8 nm cannot be detected by this gas.

Based on the gas molecule size/diffusion, it can be resumed that H_2 is the most useful gas to detect very small pores (<0.5 nm), CO_2 is the best gas to scan pores between 0.5 nm and 0.8 nm while O_2 is the most suitable to detect pores between 0.8 and 2.0 nm.

Thus, that the combination of different isotherms, by exploring only their relative pressure where the best efficacity in terms of diffusion occurs, it appears to be an interesting approach for PSD determination, as suggested elsewhere.[22,23]

Therefore, these results suggest the existence of a complex network of pores which have distinct sizes and probably various architecture and interconnectivity.

The average pore size (L_0) was determined and it can be seen (Table 1) that the size is strongly related to the adsorbate gas used. The following order can be established: $H_2 < CO_2 < O_2 < Ar < N_2$. Therefore, the H_2 can penetrate very small pores (0.52 nm), followed by CO_2 (0.94 nm) and O_2 (1.22 nm) and last, Ar and N_2 (1.45 and 1.87 nm). This indicates that all these gases are required to screen the hard carbon porosity at different levels.

Accordingly, the PSD is very distinct depending on the analysis gas, with HC behaving as a molecular sieve for adsorbed gas molecules as better illustrated by the normalized PSD (Fig. S1, ESI). This behaviour is rather different than the one observed by Jagiello et al.,[23] where the PSD derived from the adsorption of N_2 and O_2 at 77 K and Ar at 87 K were in agreement and similar. This difference can be ascribed to the nature of the carbon: activated porous carbons vs. the hard carbons used in this work. If one compares the average pore size obtain herein with the average pore size determined by SAXS analyses reported in the literature[13,24,25,32,33] on various hard carbons (Fig. S2, ESI), it can be seen that the N_2 and CO_2L_0 values falls in the same range for both techniques. However, narrow pore sizes (<0.7 nm) can be evidenced only by H_2 adsorption.

With the aim of better understanding the higher adsorption of O_2 and H_2, the isotherms were also represented as a function of the analysis time instead of the adsorbed volume (Fig. 2e and f). A very long period of time is required for O_2 to fill the micropores (~90 h). This may indicate restricted or slow diffusion of the gas through hard carbon pores, which can be associated to the very narrow pore size and probably to the specific shape of the pores (i.e., ink-bottle shape). Approximately 20 h was required for analysis of H_2 adsorption/desorption, which is significantly less time than that required for O_2 analysis.

This finding is very interesting since the adsorbed H_2 volume is rather high (82 vs. 105 $cm^3\ g^{-1}$ for O_2 at $P/P_0 = 1$) due to the very fast kinetics triggered by the smaller size of H_2 than by O_2 (0.289 vs. 0.346 nm). N_2, CO_2 and Ar exhibit the most time-efficient adsorption, with total analysis times of 3–4 h but with a limited pore accessibility and low adsorbed gas volumes.

The efficient adsorption of O_2 and H_2 can be explained by several factors that will be discussed further. First, the size of the molecule with respect to the pore size can be an important parameter to consider, with smaller molecules more easily diffusing through and accessing narrow pores. Thus, H_2, which has the smallest size (0.289 nm) among all gases and is in a supercritical state, may indeed diffuse better than other gases,[23] which would explain to some extent its high adsorbed volume. However, the molecular size of O_2 (0.346 nm) is rather similar to that of Ar (0.340 nm) and N_2 (0.364 nm), which suggests that the better adsorption of oxygen into carbon pores is not linked to its molecular size. Second, the gas quadrupole moment is known to play a role in the interactions of the gas adsorbate with carbon surface groups, i.e., orientation of the adsorbed molecule on the adsorbent surface and modification of the micropore filling pressure. According to Table 1, the order of the quadrupole moment is the following: $Ar < O_2 < H_2 < N_2 < CO_2$. We note that O_2 has a low quadrupole moment that is similar to that of Ar; thus, unlike CO_2, O_2 is expected to exhibit limited interactions with the carbon surface. Consequently, the quadrupole moment cannot explain the observed high adsorbed volumes of O_2. Third, the polarizability is used by some authors[27] to explain the increase in the adsorbed gas volume considering that it might favour adsorbent–adsorbate interactions. The polarizability order of the probe molecules is as follows: $CO_2 > N_2 > Ar > O_2 > H_2$ (Table 1). We can see that CO_2 has the highest value, while O_2 and H_2 have the lowest; therefore, fewer interactions are expected with O_2 and H_2. Once again, polarizability can be excluded as a pertinent parameter for explaining the affinity of oxygen for the carbon network. Last, the diffusivity of the gas molecules through the carbon material may impact their

adsorption capacities and kinetics. The diffusivity of O_2 has been reported to be much higher than that of N_2 or Ar,[34,35] which could also explain the enhanced adsorption of oxygen observed in this work. Nevertheless, to shed light on the precise reasons for the peculiar behaviour of O_2, more in-depth studies are required.

From a more practical point of view, it is important to address the dependence of the texture and the electrochemical properties by considering different gas molecules. We can see that the surface areas of the three HCs (HPR-1300, HAB-1300 and TCA-1400) determined with N_2 are small and very similar (~20 m^2 g^{-1}), while the surfaces determined with CO_2 or O_2 are significantly larger (up to 431 m^2 g^{-1}). The electrochemical performance of the hard carbon materials were reported in our recent works[30,36] and are briefly summarized in Table S1 (ESI). The materials show an irreversible capacity of 21%, 23% and 32% for HPR-1300, HAB-1300 and TCA-1400, respectively. These results cannot be explained only considering the N_2 SSA, as it is rather similar for all materials. However, very interestingly, this difference can be better correlated with the O_2 (or CO_2) SSAs. The O_2 SSA varies in the same order as the HCs irreversibility: 90, 181 and 431 m^2 g^{-1}. Although other parameters, such as oxygen-containing functional groups, may impact the irreversible capacity, this seems to affect less the irreversible capacity than the specific surface area as illustrated by HPR-1300 material. The later one presents more than double amount of oxygen in the structure compared to HAB-1300 (6.6 vs. 2.9 at%, Table S1, ESI) but its irreversible capacity is smaller. The higher O_2 SSA of HAB-1300 leads thus to more important irreversible capacity.

Therefore, it appears that the textural properties are very important in dictating the irreversible capacity. Usually, the electrolyte decomposition due to the carbon surface area is the most common phenomena inducing the SEI layer formation,[18] responsible partly for the high irreversible capacity during the first charge/discharge cycle. In addition, Na trapping into the narrow/restricted pores can also contribute to irreversibility.

For instance, the unsolvated ionic radius of Na^+ is about 0.102 nm, while the sizes of the EC and DMC solvent molecules are 0.342 nm and 0.441 nm.[37] If solvation shell of Na^+ is considered, the hydrodynamic radius and the diameter would be much higher, i.e., 0.35 nm and 0.70 nm, respectively. Regarding, the PF_6^- anion, its size is 0.50 nm.[38] Therefore, the size of the electrolyte molecules is smaller or comparable to that of the available pores and Na trapping cannot be neglected. Particularly, the diversity of carbon pore size may act as a molecular sieve for these different ions. However, more deep investigations are required to precisely identify

the role of each type of pore, the solvation state of Na^+ during the adsorption/charging process and the accessibility of electrolyte/solvent molecules through the pores.

In summary, the efficiency of applying non-conventional gases, such as O_2 and H_2, to reveal the porosity of hard carbons that is otherwise inaccessible to conventional gases (N_2, Ar), was demonstrated. Based on this study, we recommend that porosity evaluation of hard carbons to be performed with gases such as O_2, H_2 or CO_2 instead of N_2 or Ar. Only systematic implementation of these gases for texture evaluation will allow to adjust the hard carbon properties, to properly understand the mechanism of Na^+ storage and finally, to improve the performance of these materials. H_2 and O_2 were shown to be powerful probe molecules for determining the hard carbon texture and can be further implemented for the characterization of other materials exhibiting restricted pore size distribution, such as biochars, molecular sieves, and metal molecular frameworks.

Conflicts of interest

There are no conflicts to declare.

Acknowledgements

This work was performed in the frame of RS2E (French research network on electrochemical energy storage). The project received funding from the European Union's Horizon 2020 research and innovation program under grant agreement no. 875629. The authors acknowledge Dr Jacek Jagiello form Micromeritics for providing SAIEUS v3.2 software and for useful discussion regarding pore size distribution determination.

Notes and references

1. X. L. Chen, R. Paul and L. M. Dai, Natl. Sci. Rev., 2017, 4, 453–489
2. E. Irisarri, A. Ponrouch and M. R. Palacin, J. Electrochem. Soc., 2015, 162, A2476–A2482
3. E. Lam and J. H. T. Luong, ACS Catal., 2014, 4, 3393–3410
4. M. Sevilla and A. B. Fuertes, Energy Environ. Sci., 2011, 4, 1765–1771
5. R. K. Thines, N. M. Mubarak, S. Nizamuddin, J. N. Sahu, E. C. Abdullah and P. Ganesan, J. Taiwan Inst. Chem. Eng., 2017, 72, 116–133.
6. X. Wu, Y. L. Chen, Z. Xing, C. W. K. Lam, S. S. Pang, W. Zhang and Z. C. Ju, Adv. Energy Mater., 2019, 9, 1900343
7. X. Dou, I. Hasa, D. Saurel, C. Vaalma, L. Wu, D. Buchholz, D. Bresser, S. Komaba and S. Passerini, Mater. Today, 2019, 23, 87–104.
8. H. Hou, X. Qiu, W. Wei, Y. Zhang and X. Ji, Adv. Energy Mater., 2017, 7, 1602898
9. D. Saurel, B. Orayech, B. Xiao, D. Carriazo, X. Li and T. Rojo, Adv. Energy Mater., 2018, 8, 1703268

10. J. R. Dahn, W. Xing and Y. Gao, Carbon, 1997, 35, 825–830
11. Y. Q. Li, Y. X. Lu, Q. S. Meng, A. C. S. Jensen, Q. Q. Zhang, Q. H. Zhang, Y. X. Tong, Y. R. Qi, L. Gu, M. M. Titirici and Y. S. Hu, Adv. Energy Mater., 2019, 9, 1902852
12. C. Matei Ghimbeu, J. Górka, V. Simone, L. Simonin, S. Martinet and C. Vix-Guterl, Nano Energy, 2018, 44, 327–335
13. Y. Morikawa, S. Nishimura, R. Hashimoto, M. Ohnuma and A. Yamada, Adv. Energy Mater., 2020, 10, 1903176
14. S. Qiu, L. Xiao, M. L. Sushko, K. S. Han, Y. Shao, M. Yan, X. Liang, L. Mai, J. Feng, Y. Cao, X. Ai, H. Yang and J. Liu, Adv. Energy Mater., 2017, 7, 1700403
15. B. Zhang, C. M. Ghimbeu, C. Laberty, C. Vix-Guterl and J.-M. Tarascon, Adv. Energy Mater., 2016, 6, 1501588
16. W. Xing, J. S. Xue and J. R. Dahn, J. Electrochem. Soc., 1996, 143, 3046–3052.
17. V. Simone, A. Boulineau, A. de Geyer, D. Rouchon, L. Simonin and S. Martinet, J. Energy Chem., 2016, 25, 761–768
18. C. Bommier, W. Luo, W.-Y. Gao, A. Greaney, S. Ma and X. Ji, Carbon, 2014, 76, 165–174.
19. E. R. Buiel, A. E. George and J. R. Dahn, Carbon, 1999, 37, 1399–1407.
20. M. Thommes and K. A. Cychosz, Adsorption, 2014, 20, 233–250.
21. M. Thommes, K. Kaneko, A. V. Neimark, J. P. Olivier, F. Rodriguez-Reinoso, J. Rouquerol and K. S. W. Sing, Pure Appl. Chem., 2015, 87, 1051–1069
22. J. Jagiello and J. Kenvin, J. Colloid Interface Sci., 2019, 542, 151–158.
23. J. Jagiello, J. Kenvin, C. O. Ania, J. B. Parra, A. Celzard and V. Fierro, Carbon, 2020, 160, 164–175.
24. H. Au, H. Alptekin, A. C. S. Jensen, E. Olsson, C. A. O'Keefe, T. Smith, M. Crespo-Ribadeneyra, T. F. Headen, C. P. Grey, Q. Cai, A. J. Drew and M. M. Titirici, Energy Environ. Sci., 2020, 13, 3469–3479.
25. E. Olsson, J. Cottom, H. H. Au, Z. Y. Guo, A. C. S. Jensen, H. Alptekin, A. J. Drew, M. M. Titirici and Q. Cai, Adv. Funct. Mater., 2020, 30, 1908209.
26. D. Stevens and J. R. Dahn, J. Electrochem. Soc., 2001, 148, A803–A811.
27. P. Rallapalli, K. P. Prasanth, D. Patil, R. S. Somani, R. V. Jasra and H. C. Bajaj, J. Porous Mater., 2011, 18, 205–210.
28. C. Lynga, A. Lhuillier and C. G. Wahlstrom, J. Phys. B: At., Mol. Opt. Phys., 1996, 29, 3293–3302.
29. J. Jagiello and J. Olivier, Carbon, 2013, 55, 70–80.
30. A. Beda, P.-L. Taberna, P. Simon and C. Matei Ghimbeu, Carbon, 2018, 139, 248–257.
31. C. Matei Ghimbeu, B. Zhang, A. Martinez de Yuso, B. Rety and J.-M. Tarascon, Carbon, 2019, 153, 634–647.
32. A. Kamiyama, K. Kubota, T. Nakano, S. Fujimura, S. Shiraishi, H. Tsukada and S. Komaba, ACS Appl. Energy Mater., 2020, 3, 135–140.
33. M. Dahbi, M. Kiso, K. Kubota, T. Horiba, T. Chafik, K. Hida, T. Matsuyama and S. Komaba, J. Mater. Chem. A, 2017, 5, 9917–9928.
34. Y. Hua Ma, W. Sun, M. Bhandarkar, J. Wang and G. Miller, Sep. Technol., 1991, 1, 90–98.
35. K. P. Travis, Mol. Phys., 2002, 100, 2317–2329.
36. A. Beda, F. Rabuel, M. Morcrette, S. Knopf, P. L. Taberna, P. Simon and C. Matei Ghimbeu, J. Mater. Chem. A, 2021, 10.1039/D0TA07687B .
37. S. Amara, J. Toulc'Hoat, L. Timperman, A. Biller, H. Galiano, C. Marcel, M. Ledigabel and M. Anouti, Chemphyschem, 2019, 20, 581–594.
38. K. Kato, M. T. E. Rodrigues, G. Babu and P. M. Ajayan, Electrochim. Acta, 2019, 324, 134871.